

Complete Reaction Mechanism of Indoleamine 2,3-Dioxygenase as Revealed by QM/MM Simulations

Luciana Capece,^{†,II} Ariel Lewis-Ballester,[‡] Syun-Ru Yeh,[‡] Dario A. Estrin,^{*,†} and Marcelo A. Martí^{*,†,§}

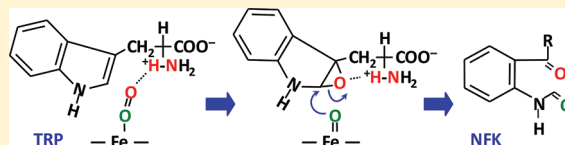
[†]Departamento de Química Inorgánica, Analítica y Química Física/INQUIMAE-CONICET, Facultad de Ciencias Exactas y Naturales, Universidad de Buenos Aires, Ciudad Universitaria, Pabellón 2, Buenos Aires, C1428EHA, Argentina

[‡]Department of Physiology and Biophysics, Albert Einstein College of Medicine, 1300 Morris Park Avenue, Bronx, New York 10461, United States

[§]Departamento de Química Biológica, Facultad de Ciencias Exactas y Naturales, Universidad de Buenos Aires, Ciudad Universitaria, Pabellón 2, Buenos Aires, C1428EHA, Argentina

Supporting Information

ABSTRACT: Indoleamine 2,3-dioxygenase (IDO) and tryptophan dioxygenase (TDO) are two heme proteins that catalyze the oxidation reaction of tryptophan (Trp) to *N*-formylkynurenine (NFK). Human IDO (hIDO) has recently been recognized as a potent anticancer drug target, a fact that triggered intense research on the reaction and inhibition mechanisms of hIDO. Our recent studies revealed that the dioxygenase reaction catalyzed by hIDO and TDO is initiated by addition of the ferric iron-bound superoxide to the C₂=C₃ bond of Trp to form a ferryl and Trp—epoxide intermediate, via a 2-indolenylperoxy radical transition state. The data demonstrate that the two atoms of dioxygen are inserted into the substrate in a stepwise fashion, challenging the paradigm of heme-based dioxygenase chemistry. In the current study, we used QM/MM methods to decipher the mechanism by which the second ferryl oxygen is inserted into the Trp—epoxide to form the NFK product in hIDO. Our results show that the most energetically favored pathway involves proton transfer from Trp—NH₃⁺ to the epoxide oxygen, triggering epoxide ring opening and a concerted nucleophilic attack of the ferryl oxygen to the C₂ of Trp that leads to a metastable reaction intermediate. This intermediate subsequently converts to NFK, following C₂—C₃ bond cleavage and the associated back proton transfer from the oxygen to the amino group of Trp. A comparative study with *Xantomonas campestris* TDO (xcTDO) indicates that the reaction follows a similar pathway, although subtle differences distinguishing the two enzyme reactions are evident. The results underscore the importance of the NH₃⁺ group of Trp in the two-step ferryl-based mechanism of hIDO and xcTDO, by acting as an acid catalyst to facilitate the epoxide ring-opening reaction and ferryl oxygen addition to the indole ring.



Indoleamine 2,3-dioxygenase (IDO) and tryptophan dioxygenase (TDO) are two heme-based dioxygenases that catalyze the oxidative ring-cleavage reaction of tryptophan (Trp) to *N*-formylkynurenine (NFK), the initial and rate-limiting step of the kynurenine pathway.^{1–8} Human IDO (hIDO) is inducible by interferon- γ and is expressed in all tissues.⁹ It functions as an immuno-suppressor and is linked to a variety of immune-related physiological and pathophysiological conditions. Mammalian, and particularly Human TDO (hTDO), on the other hand, is mostly expressed in the liver and is responsible for regulating Trp flux.^{2,6,10} Recently, IDO was shown to promote immune escape of cancer;^{11–15} in this context, in cooperation with chemotherapeutic agents, an IDO inhibitor (1-methyl Trp) was found to facilitate regression of established tumors in mice,¹² underscoring the potential of IDO inhibitors in cancer therapy. The recognition of IDO as a potent anticancer drug target has triggered intense research on the reaction and inhibition mechanisms of IDO, as well as TDO.^{16–21}

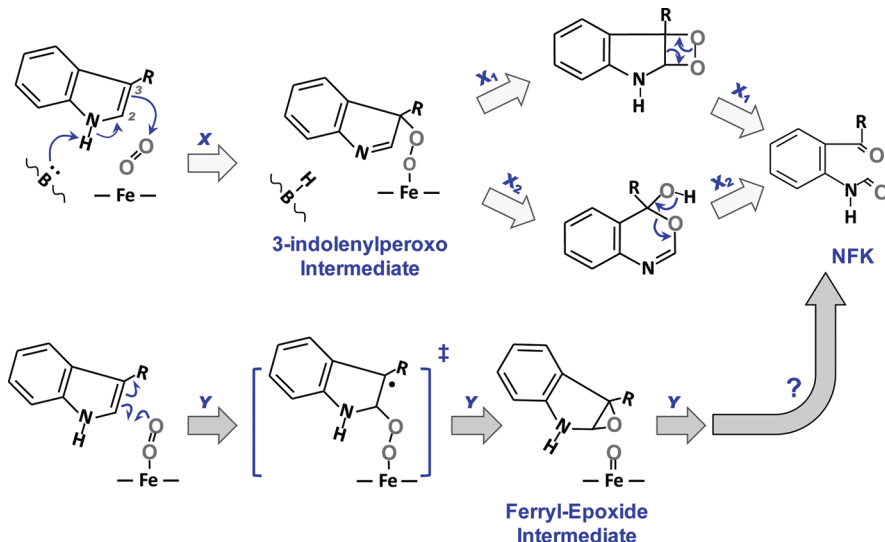
Both IDO and TDO have been extensively characterized from a biochemical,^{1,2,7,18,22} spectroscopic,^{3,4,16,19,23–25} and structural perspective.^{5,6,17,26,27} A recent review on structural and mechanistic issues has been published by Basran and Raven.²⁸ Although

the crystal structure of hTDO has not been obtained yet, structural data of two bacterial isoforms of TDO from *Cupriavidis metalodurians* and *Xantomonas campestris* (CmTDO and xcTDO, respectively)^{5,6,26} show that TDO is a tetrameric enzyme, with one heme per monomer. On the other hand, the crystal structure of hIDO shows that it is a monomeric enzyme, and even though these two enzymes exhibit low sequence homology, structure-based sequence alignment reveals a high structural similarity between them. Despite intense research during the past few decades, the mechanism by which oxygen is inserted into Trp by IDO and TDO remained elusive. Nonetheless, as most of the critical residues involved in the substrate—protein interactions found in TDO are conserved in IDO,^{6,26} it was generally believed that the two classes of dioxygenases catalyze the reaction by a similar mechanism.^{2,29} In the widely believed base-catalyzed mechanism first proposed by Hamilton, the reaction is initiated by deprotonation of the indoleamine group of Trp by an active site base that triggers the electrophilic addition of heme-bound

Received: August 26, 2011

Revised: December 22, 2011

Published: December 23, 2011

Scheme 1. Proposed Dioxygenase Mechanisms Catalyzed by IDO and TDO^a

^a Mechanisms X₁ and X₂ correspond to the dioxetane and Criegee rearrangement mechanisms, respectively. Mechanism Y is adapted from our earlier work.^{16,20}

dioxygen to the C₂=C₃ bond of the deprotonated Trp, leading to a heme-bound 3-indolenylperoxo intermediate. This intermediate subsequently converts to the product, NFK, via a dioxetane intermediate or Criegee-type rearrangement, as illustrated by pathways X₁ and X₂ in Scheme 1, respectively.^{2,8,29}

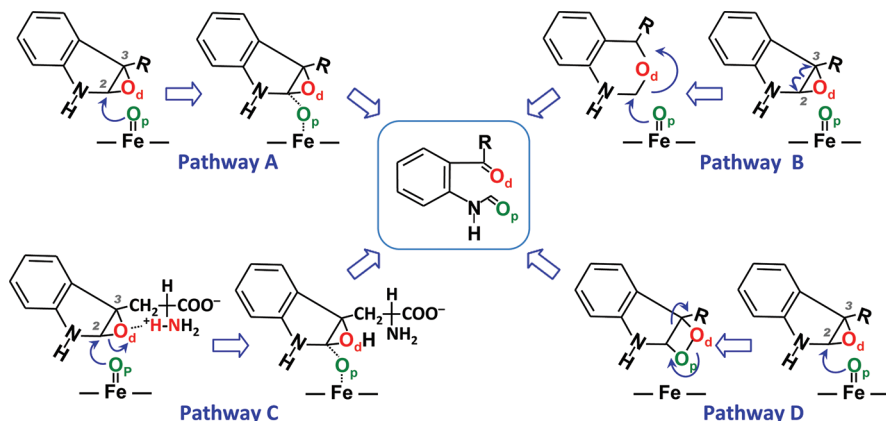
Partial support for the base-catalyzed mechanism came from: (1) chemical studies of the oxidation reaction of Trp by singlet oxygen in water, which revealed the 3-indolenylperoxo and dioxetane³⁰ intermediates, and (2) crystallographic studies of xcTDO, which showed a strong hydrogen bond between the indoleamine group of Trp and a nearby residue, H55, hinting that this residue is the active site base that triggers the reaction in TDO.³ Structural-based sequence alignment shows that the position of H55 in xcTDO is occupied by S167 in hIDO. Structural studies also showed that S167 is not able to interact with bound Trp.^{17,26} On this basis, the active site base in hIDO was proposed to be the heme-bound dioxygen.^{3,24,26} Although convincing, the following new evidence casted doubts on the base-catalyzed mechanism: (1) site-directed mutagenesis studies of TDO showed that the replacement of H55 in hTDO or H76 (equivalent to H55 in xcTDO) by Ala does not completely abolish the Trp oxidation activity,^{4,7,27} (2) significant hIDO activity was observed when the physiological substrate Trp was replaced by 1-methyl Trp (in which the indoleamine moiety is methylated),^{18,22} and (3) computational studies of a O₂-indole-heme model system in vacuum showed that proton transfer from indoleamine to the heme-bound dioxygen and the associated dioxygen insertion into the substrate exhibit a very high activation barrier³¹ (an observation that was later confirmed for hIDO and xcTDO dioxygenase reaction by Quantum Mechanics/Molecular Mechanics (QM/MM) studies carried out by us and others).^{20,32,33}

In line with the above-mentioned evidence, using a combined experimental and computational approach,^{16,20} we revealed and corroborated several important features of the reaction: (1) neither H55 in xcTDO nor heme-bound dioxygen in hIDO is able to deprotonate the indoleamine group of Trp, (2) the

ternary complexes of hIDO and xcTDO are activated by partial electron transfer from the heme to the dioxygen, as evident by the superoxide character of the heme-bound dioxygen (indicated by the ν_{O–O} at 1137 cm⁻¹),¹⁶ consistent with the previous proposal by Brady and Feigelson for TDO,³⁴ and (3) the activated superoxide is inserted into the C₂=C₃ bond of Trp to form a 2-indolenylperoxo radical transition state, which triggers the O–O bond cleavage reaction, leading to a ferryl and Trp–epoxide intermediate,^{16,20} as summarized in Pathway Y in Scheme 1. It is noteworthy that the presence of the ferryl intermediate in hIDO was later confirmed by Yanagisawa et al.²⁵ In addition, a similar ferryl derivative was identified in CmTDO during its reaction with H₂O₂ by Fu et al.,³⁵ while the Trp–epoxide intermediate has been indirectly inferred by Basran et al.²¹ from a cyclic amino acetal side product derived from the dioxygenase reaction of hIDO, xcTDO, and hTDO.²¹ Therefore, although there is significant evidence confirming the existence of the ferryl and Trp–epoxide intermediate, both dioxygenases, how this intermediate state proceeds to NFK in hIDO is still not completely understood.

To map out the second oxygen insertion reaction in hIDO, associated with the conversion of the ferryl and Trp–epoxide intermediate to the NFK product, in the present work we have performed QM/MM studies of several potential mechanistic pathways, as illustrated in Scheme 2. In the first path, the reaction is initiated by direct nucleophilic attack of the ferryl oxygen to the C₂ atom (Pathway A), while in the second path the reaction is initiated by homolytic C₂–C₃ bond cleavage induced ring expansion, coupled with the nucleophilic attack of the ferryl oxygen to the C₂ atom (Pathway B). In Pathway C, the reaction is initiated by proton transfer (from Trp–NH₃⁺ to the epoxide oxygen) assisted epoxide ring opening, coupled with nucleophilic addition of the ferryl oxygen to the C₂ of Trp. This pathway was hypothesized based on the observation that in the ferryl and Trp–epoxide intermediate the epoxide oxygen (O_d) forms a H-bond with Trp–NH₃⁺ and the fact that the ring-opening reaction of epoxides is known to be facilitated by protonation of

Scheme 2. Four Potential Pathways Leading from the Ferryl and Trp-Epoxyde Intermediate to the Product NFK: (A) Nucleophilic Addition Reaction, (B) Ring-Expansion Coupled with Nucleophilic Addition Reaction, (C) Proton Transfer-Assisted Ring-Opening Reaction Coupled with Nucleophilic Addition Reaction, and (D) Dioxetane-Mediated Mechanism



the epoxide oxygen. In pathway D, the reaction is mediated by a dioxetane intermediate derived from direct nucleophilic attack of the ferryl oxygen to the C₂ atom. As a reference, we also evaluated the possibility of generating the dioxetane intermediate directly from the ternary complex. All pathways were evaluated in hIDO in both singlet (S) and triplet (T) spin states (in some cases the quintet (Q) state was considered as well). The results indicate that the reaction is best described by Pathway C, which exhibits the lowest energy barrier for the second oxygen insertion. For comparison purposes, pathway C has also been evaluated for xcTDO. The results on xcTDO indicate that xcTDO and hIDO follow similar mechanisms, but subtle differences distinguishing the two enzyme reactions are evident.

■ COMPUTATIONAL METHODS

The structures and methods used in the present work are the same as those published previously in our previous studies of the first oxygen insertion step for the hIDO and xcTDO reactions.^{16,20} The initial structure of the ternary complex of hIDO (i.e., oxygenated and with L-Trp bound) used for the previous and present studies was obtained by docking the substrate L-Trp to the crystal structure of the substrate-free enzyme (PDB: 2D0T)²⁶ which was further analyzed and relaxed using Molecular Dynamics (MD).

Briefly, the docking protocol consisted of performing 100 flexible ligand docking runs (using Autodock)³⁶ for a set of 10 selected IDO structures, obtained from MD simulations. The resulting structures were analyzed and clustered into groups of possible complex conformations, which showed the presence of two major clusters for the hIDO L-Trp complex. The first conformation (L-Cf1) appeared in 44% of cases. This conformation was selected as the starting point for MD simulations used to obtain the corresponding QM/MM starting structures as described below. All MD simulations were performed using the PMEMD module of the Amber9 package.³⁷ Further details and analysis of the docking results can be found in previous work from our group.¹⁷

For xcTDO the structure corresponds to a one-subunit model of TDO, which contains all residues of subunit A, but the first 15 residue helix (D19 to S35) which penetrates the other subunit, plus residues R21 to S35 of subunit B, that was constructed based

on the available L-Trp-bound crystal structure (PDB: 2NW8) and which was also subjected to MD in the ternary complex.¹⁷

All classical molecular dynamics simulations were performed in explicit water with previously reported parameters.³⁸ Standard protonation states at physiological pH were assigned to ionizable residues. Special attention was paid to the protonation states of histidines, which were assigned on the basis of the hydrogen bonding patterns with neighboring residues. For hIDO, the proximal histidine (H346) and H73 were simulated in the HID tautomeric state (i.e., with proton in the delta nitrogen), while all other histidine residues were simulated in the HIE tautomeric state (i.e., with proton in the epsilon nitrogen). For xcTDO, the proximal histidine (H240), H55, and H75 were considered in the HID protonation state, whereas all the other histidine residues were simulated in the HIE state.

For each protein ternary complex, after cooling to 0 K using MD, hybrid QM/MM calculations were used to study the first oxygen insertion that leads to the ferryl and Trp-epoxide intermediate.^{16,20} This ferryl and Trp-epoxide intermediate was used as the starting structure in the present work. All QM/MM calculations were performed at the DFT level using the SIESTA code with our own QM/MM implementation called Hybrid.³⁹ For all atoms, basis sets of double- ζ plus polarization quality were employed; all calculations were performed by using the generalized gradient approximation functional proposed by Perdew, Burke, and Ernzerhof (PBE).⁴⁰ For all systems studied, the spin-unrestricted approximation was used unless explicitly noted. The QM subsystem included the heme group (without the peripheral groups), the O₂, the substrate (L-Trp), and the imidazole group of the proximal histidine. For xcTDO, the imidazole group of H55 was also included in the QM subsystem. The rest of the protein and the water molecules were treated classically. QM/MM methods have been successfully applied for the study of enzyme reactions including heme proteins.^{41–43} Particularly, the Hybrid method showed excellent performance for medium and large systems and was proven to be appropriate for biomolecules, specifically heme proteins, as shown by several works from our group.^{39,44–47}

Since obtaining accurate free energy profiles requires extensive sampling, which is computationally very expensive and difficult to achieve at the DFT QM/MM level, we resorted to computing potential energy profiles by using restrained energy minimizations

along the reaction path that connects reactant and product states.^{39,48,49} For this approach, an additional term, $V(\xi) = k(\xi - \xi_0)^2$, is added to the potential energy, where k is an adjustable force constant (set to be 200 kcal/mol·Å²) and ξ_0 is a reference value, which is varied stepwise along the reaction coordinate. By varying ξ_0 , the system is forced to follow the energy minimum reaction path along the given reaction coordinate ξ . This methodology has been widely used by our group in various studies.^{39,50}

By using different reaction coordinates (ξ), we were able to analyze the different pathways shown in Scheme 2. It is important to note that even for a complex reaction mechanism as the one observed in xcTDO (vide infra) very similar results are obtained with slightly different reaction coordinates (see Figure 5 versus Figure S3 in the Supporting Information), provided that the chosen reaction coordinate is capable of sampling the correct geometrical parameters. This fact underscores the reliability of the applied strategy.

To validate the optimized structures for all relevant proposed intermediates and transition states, we performed state of the art Hessian calculations. The calculations were performed by computing for each structure the second force derivative matrix for just the QM subsystem, using the Gaussian03 program.⁵¹ Diagonalization of the matrix yields the corresponding eigenvalues which correspond to each mode frequency (in cm⁻¹), while the eigenvector represents the motion of the system along the mode. Relevant modes (i.e., imaginary frequency modes for TS or Fe–X stretching frequencies) were visually analyzed. As expected, we found one imaginary frequency corresponding to the reaction mode for each TS, while all intermediate states, reactants, and products displayed only positive frequencies.

To test the effect of the functional on the obtained results and to be able to perform a straightforward comparison between the present results and those previously obtained for xcTDO,^{33,52} we performed selected validation calculations using the B3LYP functional with the Gaussian03 program.⁵¹ The results indicate that the predicted mechanism and obtained barriers are very similar to those calculated with Hybrid for both enzymes and therefore do not depend significantly on the functional choice, although minor differences are observed and discussed especially concerning the first step. For comparison purposes, we also computed again the first oxygen insertion step using the B3LYP functional. Although, the results shown in the Supporting Information are similar to those obtained with PBE, it should be noted that for the first oxygen insertion Chung et al.³³ obtained a two-step mechanism with a ferric superoxide intermediate, while we have obtained a concerted first oxygen insertion with both PBE and B3LYP functionals and in both enzymes. It is possible that the origin of this difference arises from the use of slightly different optimized structures. In ref 33, snapshots for QM/MM optimization were directly taken from 300 K production runs, while in our case the system was initially cooled slowly to 0 K before QM/MM optimization. In our long experience, slow cooling protocols lead to a better and more representative structure (i.e., closer to the global minima) since structures taken directly from 300 K MD simulation runs and QM/MM optimized may be trapped in local minima that do not correspond to the best structure. Also important may be the fact that we used a truncated monomeric model of xcTDO. More details about the computational methods can be found in the Supporting Information.

Table 1. Structural and Electronic Properties of the Ferryl and Trp–Epoxide Intermediate in the S, T, and Q States for hIDO and the T State for xcTDO^a

spin state	hIDO			xcTDO
	S	T	Q	T
ΔE_{Spin}	7.7	0.0	17.3	0.0
dC_2-O_p	2.972	3.021	2.990	3.001
$dFe-O_p$	1.668	1.679	1.667	1.667
qC_2	0.117	0.115	0.120	0.072
qO_d	-0.210	-0.204	-0.211	-0.199
qO_p	-0.354	-0.360	-0.372	-0.348
qFe	0.799	0.806	1.010	0.797
$qTrp\text{--epoxide}$	0.063	0.064	0.061	-0.317
spin O_p	0.001	0.824	0.678	0.824
spin Fe	0.001	1.252	3.072	1.225
spin heme moiety	-0.001	1.994	3.995	1.993
spin Trp–epoxide	0.001	0.006	0.005	0.007

^a ΔE_{Spin} corresponds to the relative energy of each spin state with respect to the T state (ground state). Spin of the heme moiety corresponds to the Mulliken spin population of the heme ferryl species, including the iron porphyrin, the oxygen, and its proximal histidine ligand. The energies, distances, and charges/spin densities are in kcal/mol, angstroms, and e units, respectively.

RESULTS

In the following section, we first describe the electronic structure of the ferryl Trp–epoxide intermediate of hIDO and xcTDO resulting from the initial oxygen insertion reaction and summarize the energetic barrier and structural results obtained for the different pathways illustrated in Scheme 2. We then describe the details of the most energetically feasible pathway, pathway C, followed by a brief description of the less favored mechanisms, corresponding to pathways A, B, and D (Scheme 2). The energetic barrier and structural data obtained from the different pathways illustrated in Scheme 2 are summarized in Tables 1–4. Finally, we evaluate pathway C for xcTDO and compare the results with those obtained for hIDO. For all cases, reactions are analyzed along the T state since it corresponds to the ground state of the starting ferryl–Trp–epoxide complex, while the energetic parameters associated with the corresponding reactions are studied not only in the T state but also in the S and Q states.

Ferryl and Trp–Epoxide Intermediate. Our previous QM/MM studies showed that the ternary complex of hIDO has an open-shell singlet (S) ground state, which is close in energy to the triplet (T) state ($\Delta E = 0.6$ kcal/mol) and with the heme-bound O₂ in superoxide configuration.^{16,20,25} The first oxygen insertion reaction proceeds similarly in both S and T states, leading to the ferryl and Trp–epoxide intermediate (Pathway Y in Scheme 1) and displaying barriers of 15.5 and 13.8 kcal/mol, respectively. The first oxygen insertion is clearly exothermic with the intermediate lying below the ternary complex. Our previous data also show that equivalent results were obtained for the first oxygen insertion step in xcTDO, with an even smaller barrier of 8.1 kcal/mol (in the T state). These results are summarized in Table 2.

The structural and electronic parameters of the ferryl Trp–epoxide intermediate are summarized in Table 1. For hIDO, the ferryl moiety has a T ground state, similar to that found in compound II of peroxidases.⁵³ The T state, with the unpaired

spin completely localized in the Fe=O moiety, is 7.7 kcal/mol lower in energy, as compared to the S state. The Q state, on the

Table 2. Activation and Spin Gap Energies for the Various Reaction Pathways Examined in This Work, In the S, T, and Q States^a

mechanism	hIDO		xcTDO
	spin state		
	S	T	Q
$\Delta E^\#$ (first oxygen insertion)	15.5	13.8	n.c.
ΔE (first oxygen insertion)	-9.2	-16.2	n.c.
pathway A	32.0	32.7	-
pathway B(1)	31.8	31.5	-
pathway B(2)	29.4	30.5	-
pathway C	21.4	20.7	20.0
pathway D	≥ 34	≥ 36	≥ 26
$\Delta E_{\text{reaction}}$	-36.3	-31.7	-31.8
$\Delta E_{\text{spin NFK}}$	0	4.6	11.5
			5.9 ^b

^a For each pathway (labeled as A, B(1), B(2), C, and D), we report the energy barrier for the second oxygen insertion step relative to the ferryl Trp–epoxide complex in the corresponding spin state. Pathways B(1) and B(2) correspond to alternative reaction coordinates for pathway B in Scheme 2 (see below for further details). $\Delta E^\#$ (first oxygen insertion) and ΔE (first oxygen insertion) correspond to the activation barrier and the energy change for the first oxygen insertion step determined in our previous work.²⁰ $\Delta E_{\text{spin NFK}}$ corresponds to the relative energy of NFK in each spin state with respect to that of the ground state. $\Delta E_{\text{reaction}}$ is the relative energy of the product NFK, with respect to the ferryl–epoxide intermediate. All the values are given in kcal/mol. ^b The ground state of xcTDO in complex with NFK also corresponds to the S state.

other hand, is significantly higher in energy. The localization of the unpaired spin population for the S state is similar to that found by Derat et al.⁵⁴ for compound II of horse radish peroxidase, in vacuum and using B3LYP, which shows an unpaired spin population of the Fe and O atoms of 1.23 and 0.95 e, respectively. Interestingly, in the S state in our case the systems adopt a closed-shell state, while the results of Derat et al. show that the spin populations are 0.47 and -0.43 for the Fe and O atoms, respectively. These results correspond to an intermediate between a completely closed-shell state (as found in the present case) and an open-shell ground state (as found for the ternary Fe–O₂ complex) where the spin populations are close to 1.0 and -1.0 for the Fe and the O, respectively. The origin of this difference is not clear and could be due to the presence of the enzyme (Derat et al.⁵⁴ calculations were done in vacuum) or due to the use of a different computational setup.

Müllerken charge population analysis shows that charge distributions are similar in all spin states. Both the ferryl moiety (including the proximal histidine and the ferryl heme) and the Trp–epoxide are almost neutral, although the Fe=O bond is highly polarized with the oxygen (O_p) bearing a significant negative charge (<-0.35e). In the Trp–epoxide, the oxygen (O_d) is slightly negative, and therefore the adjacent carbon C₂ is slightly positive. The distance between C₂–O_p is ~3 Å, which puts the two atoms near the van der Waals contact. To further characterize the ferryl–epoxide complex in hIDO, we computed the Fe–O stretching frequency (ν Fe=O), which resulted in 803 cm⁻¹, in excellent agreement with the frequency observed in our previous work using a resonance Raman of 799 cm⁻¹.¹⁶

To evaluate the fate of the ferryl and Trp–epoxide intermediate along the four potential reaction pathways illustrated in Scheme 2, each possible reaction energy profile was calculated

Table 3. Structural Parameters of the Transition and Intermediate States Associated with the Various Reaction Pathways Examined in This Work^a

hIDO	ferryl–epoxide ³	pathway A		pathway B(1)			pathway B(2)		
		TS _A ¹	TS _A ³	TS _{B(1)} ¹	I _{B(1)} ¹	TS _{B(1)} ³	I _{B(1)} ³	TS _{B(2)} ¹	TS _{B(2)} ³
dFe–O _p	1.68	1.97	1.85	1.68	1.71	1.68	1.68	1.76	1.77
dC ₂ –O _p	3.02	1.80	1.90	2.75	2.72	2.84	2.83	1.96	1.99
dC ₂ –C ₃	1.50	1.63	1.58	2.24	2.40	2.25	2.39	1.79	1.77
dC ₂ –O _d	1.29	1.45	1.45	1.42	1.30	1.38	1.29	1.43	1.42
pathway C									
	TS _{C(I)} ¹	I _C ¹	TS _{C(I)} ³	I _C ³	TS _{C(I)} ⁵	I _C ⁵	NFK ¹	NFK ³	NFK ⁵
dFe–O _p	1.68	1.85	1.68	1.83	1.70	1.91	2.00	2.50	2.35
dC ₂ –O _p	2.34	1.37	2.35	1.40	2.13	1.36	1.25	1.24	1.25
dC ₂ –C ₃	1.57	1.68	1.57	1.63	1.56	1.67	2.92	2.92	2.89
dC ₂ –O _d	2.36	2.47	2.33	2.42	2.38	2.47	2.43	2.41	2.32
pathway C ³									
xcTDO	ferryl–epoxide ³	TS ₁	I ₁	TS ₂	I ₂	TS ₃	NFK ¹	NFK ³	NFK ⁵
dFe–O _p	1.67	1.67	1.67	1.68	1.82	1.85	1.99	2.44	2.21
dC ₂ –O _p	3.00	2.37	2.36	1.75	1.44	1.33	1.26	1.24	1.24
dC ₂ –C ₃	1.51	1.57	1.58	1.53	1.61	2.08	2.81	2.76	2.78
dC ₂ –O _d	1.49	2.30	2.33	2.28	2.37	2.61	2.40	2.62	2.40

^a Superscripts 1, 3, or 5 indicate the values associated with the S, T, and Q states, respectively. All the values are given in Angstroms. Pathways B(1) and B(2) correspond to alternative reaction coordinates for pathway B in Scheme 2 (see below).

Table 4. Mülliken and Spin Population Analysis of the Most Relevant Transition States and Intermediates of xcTDO and hIDO Based on Pathway C, As Well As the Product NFK in the Triplet State^a

	hIDO					
	TS _{C(I)}	I _C	TS _{C(II)}	NFK		
qFe	0.835	0.890	0.892	0.941		
qC ₂	0.229	0.026	-0.004	0.068		
qO _d	-0.164	-0.143	-0.149	-0.147		
qO _p	-0.347	-0.214	-0.193	-0.148		
qN(indolic)	0.041	0.226	0.215	0.002		
qH(indolic)	-0.001	-0.006	-0.006	0.000		
qN(NH ₃ ⁺ -Trp)	0.425	0.405	0.493	0.700		
spin Fe	1.373	1.244	1.214	2.295		
spin C ₂	0.001	-0.016	0.008	-0.010		
spin O _d	0.010	0.017	0.051	-0.011		
spin O _p	0.617	0.222	0.203	0.016		
spin heme-moiety	1.995	1.994	1.950	2.001		
spin epox/NFK	0.005	0.006	0.005	-0.001		
	xcTDO					
	TS ₁	I ₁	TS ₂	I ₂	TS ₃	NFK
qFe	0.808	0.811	0.838	0.894	0.897	0.948
qC ₂	0.112	0.071	0.169	-0.008	-0.064	-0.002
qO _d	-0.217	-0.194	-0.138	-0.143	-0.172	-0.150
qO _p	-0.341	-0.328	-0.344	-0.221	-0.186	-0.117
qN(indolic)	0.366	0.435	0.416	0.402	0.406	0.366
qH(indolic)	-0.214	-0.228	-0.218	-0.212	-0.210	-0.227
qN(NH ₃ ⁺ -Trp)	0.716	0.496	0.480	0.490	0.665	0.730
spin Fe	1.258	1.267	1.294	1.086	0.999	2.288
spin C ₂	0.004	-0.004	-0.037	-0.026	0.108	-0.022
spin O _d	0.009	0.015	0.050	0.059	0.160	0.035
spin O _p	0.779	0.768	0.526	0.215	0.154	0.000
spin heme-moiety	2.002	1.995	1.932	1.922	1.832	2.003
spin Epox/NFK	-0.002	0.005	0.068	0.078	0.168	-0.003

^a qN(indolic) and qH(indolic) correspond to the Mülliken Charge Populations of the N and H atoms of the Trp indolic ring, respectively. qN(NH₃⁺-Trp) corresponds to the Mülliken Charge Population of the N atom in the Trp-NH₃⁺ group. Spin Fe, C₂, O_d, and O_p correspond to spin populations of the corresponding atoms. Spin Heme moiety corresponds to the spin of the heme ferryl species, including the iron porphyrin, the oxygen (O_d), and its proximal histidine ligand, except for the NFK column where it includes only the iron porphyrin and its proximal histidine ligand. Spin epox/NFK corresponds to the spin of the epoxide or NFK fragment. All the Mülliken charge and spin populations are given in e.

in both the S and T states (and in some selected cases also in the Q state). The results for all spin states and possible paths are summarized in Tables 2 and 3. The data clearly indicate that pathway C with a barrier of ~20 kcal/mol is the most likely mechanism, as all the other proposed mechanisms show barriers of >30 kcal/mol.

Pathway C: Proton Transfer-Assisted Epoxide Ring Opening Coupled with a Nucleophilic Ferryl Oxygen Addition Reaction. As a simple proton transfer from Trp-NH₃⁺ to epoxide does not seem to be an accessible reaction pathway, since the

barrier is greater than 20 kcal/mol, and neither a transition state nor any stable intermediate could be found (see Figure S1 in Supporting Information for details), we examined a concerted mechanism, by using [d(C₂-C₃) + d(C₂-O_d)] - [d(C₂-O_p) + d(C_α-O_d)] as the reaction coordinate. This reaction coordinate allows the system to explore the epoxide ring-opening reaction (associated with d(C₂-O_d)), together with six-membered ring formation (associated with d(C₂-C₃)) and ferryl oxygen attack to C₂ (associated with d(C₂-O_p)). It is noted that d(C_α-O_d) was initially included in the reaction coordinate to force the NH₃⁺ moiety of Trp to be close to O_d, thereby promoting the epoxide ring-opening reaction; however, the obtained results show that this distance does not fluctuate significantly along the reaction coordinate.

As shown in Figure 1, the reaction is initiated by the proton transfer from Trp-NH₃⁺ to the epoxide oxygen (O_d), which triggers the ring opening of the epoxide (blue trace in Figure 1b) and the concerted nucleophilic attack of the ferryl oxygen (O_p) to C₂ (red trace), leading to the intermediate, I_C. In the intermediate state, I_C, the proton has been transferred from Trp-NH₃⁺ to O_d; the epoxide ring is opened; and a new bond is established between C₂-O_p, while the C₂-C₃ and Fe-O_p bonds remain intact (Figure 1b). In the transition state, TS_{C(I)}, the C₂, has a sp²-like planar configuration, ready to accept the incoming O_p, in contrast to the sp³ character observed in I_C, due to the presence of the C₂-O_p bond. The intermediate, I_C, subsequently converts to the heme-bound NFK, following the C₂-C₃ bond cleavage and the associated back proton transfer from O_d-H to Trp-NH₂. The associated transition state TS_{C(II)} corresponds to a structure with an enlarged C₂-C₃ bond and in which back proton transfer has already occurred. At the end of the reaction (RC ≈ 1 Å), the potential energy surface is nearly flat. Finally, eliminating all restraints leads to the optimized NFK product (corresponding to RC ≈ 2 Å), which is described below. Further characterization of TS structures can be obtained from the frequency calculations. The results show that TS_{C(I)} displays one imaginary (negative) frequency, which corresponds to the concerted approach of the proton from the NH₃⁺ to the epoxide O_d and the O_p attack to C₂. In the TS_{C(II)} the mode with imaginary frequency involves the proton transfer from the O_d to the NH₂ and the stretching of the C₂-C₃ bond, in perfect agreement with the proposed reaction mechanism.

Consistent with the above-described mechanistic picture, Mülliken charges and spin population analysis (Table 4) show the slight development of a carbocation character on C₂ in TS_{C(I)} with respect to the Trp-epoxide complex. Additionally, the high negative charge (and unpaired spin) on the ferryl oxygen (O_p) is maintained in TS_{C(I)} but is significantly reduced at I_C (to almost half its original value), showing the C₂-O_p bond in I_C already displays the carbonyl character. Finally, the spin population analysis of the iron shows that only when NFK is completely formed (after TS_{C(II)}), and the Fe-O_p interaction is broken, the iron acquires the total unpaired spin (~2). As summarized in Tables 2 and 3, similar results were obtained for the S and even Q state reactions. As the conversion of I_C to the final NFK product is an almost barrierless process (with an activation energy <2 kcal/mol), the rate-limiting step of the reaction lies on the ferryl-Trp-epoxide → I_C transition, which exhibits an activation energy barrier of ~21 kcal/mol. The activation energy barrier is significantly lower than those of the other reaction pathways examined in this work, demonstrating that pathway C

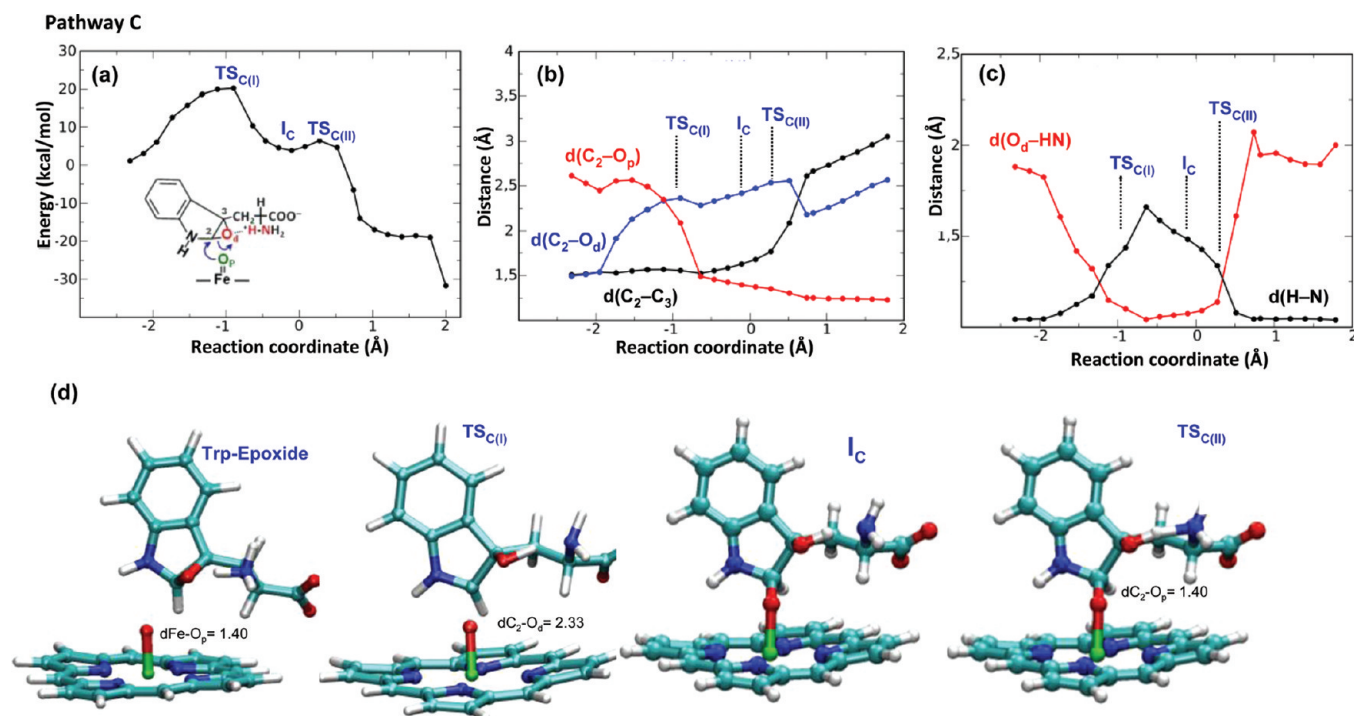


Figure 1. Energy profile (a) and distance profiles (b and c) as a function of the reaction coordinate along pathway C, as well as the structures of the epoxide intermediate, the transition state TS_{C(I)}, the intermediate I_C, and the transition state TS_{C(II)} (from left to right in panel d) in hIDO.

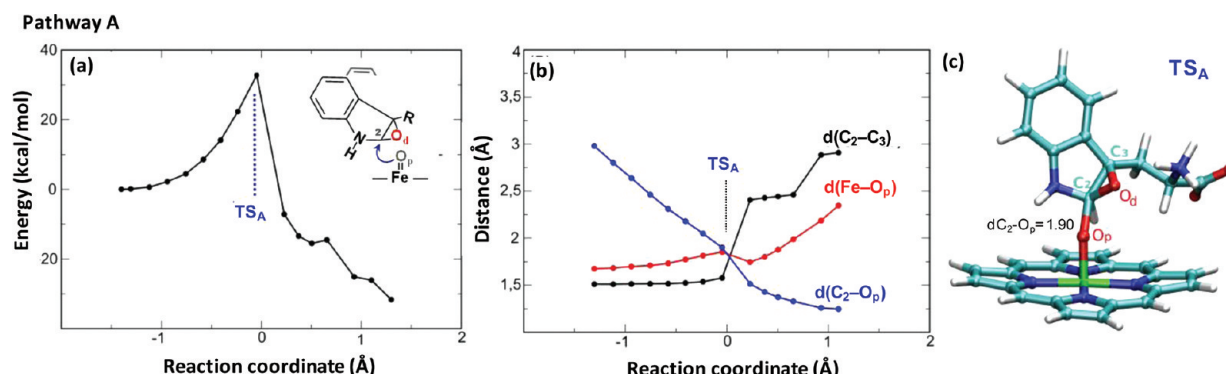


Figure 2. Energy profile (a) and distance profiles (b) as a function of the reaction coordinate along pathway A in the triplet state and the structure of the associated transition state TS_A (c).

is the energetically favored reaction pathway. In the following section we present a brief analysis of pathways A, B, and D.

Pathway A: Nucleophilic Ferryl Oxygen Addition Reaction. To test the possibility of a direct attack of the ferryl oxygen (O_p) toward C₂ of the Trp-epoxide, we computed the minimum energy trajectory of the reaction by using $d(\text{Fe}-\text{O}_p)-d(\text{C}_2-\text{O}_p)$ as the reaction coordinate. As shown in Figure 2, the reaction yields NFK, via the transition state, TS_A, in which a new C₂-O_p bond is established, while the C₂-C₃ bond is elongated (see the blue and black traces, respectively, in Figure 2b). As shown in Figure 2c, in TS_A, the C₂ has a trigonal bipyramidal structure with the C₂-O_d, C₂-H, and C₂-N bonds on almost the same plane (planar angle is 1.1°), although the axial bonds C₂-O_p and C₂-C₃ are in a bent conformation with $\angle \text{O}_p-\text{C}_2-\text{C}_3$ at $\sim 148^\circ$. In the product, NFK, the C₂-C₃ bond is completely broken, and a stable C₂-O_p bond is formed

(Figure 2b). Also, there appears to be a small metastable intermediate ($\text{RC} \approx 0.5$) followed by a second TS with a very small barrier. Visual inspection of the structures and the results in Figure 2b show that the process corresponds to a conformational rearrangement of the newly formed carbonyl groups in NFK as characterized by the enlargement of the C₂-C₃ distance. Energetic calculation shows that the reaction is highly exergonic (-32 to -39.4 kcal/mol); in addition, to reach the product the reaction has to overcome a significantly high activation energy barrier (~ 31 kcal/mol). As listed in Tables 2 and 3, the energetic parameters associated with the S and T state reaction are analogues; likewise, the structural parameters of TS_A are comparable in the two spin states.

Pathway B(1): Ring Expansion Followed by a Nucleophilic Ferryl Oxygen Addition Reaction. In pathway A, ferryl oxygen (O_p) addition to C₂ precedes the C₂-C₃ bond cleavage.

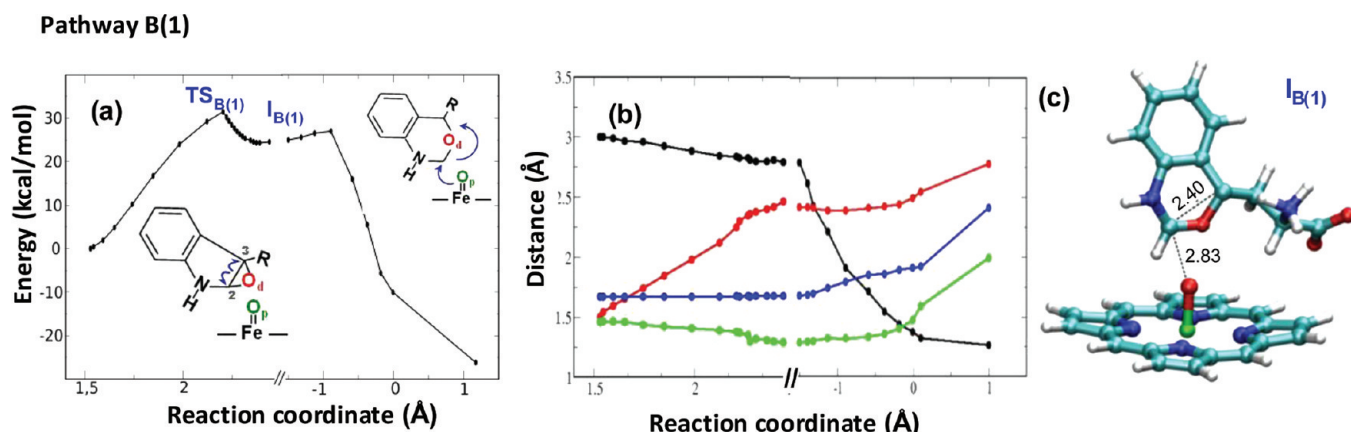


Figure 3. Energy profile (a) and distance profiles (b) as a function of the reaction coordinate along pathway B(1) in the triplet state and the structure of the associated intermediate $I_{B(1)}$ (c). The // symbol in the x -axis indicates the change in the reaction coordinate.

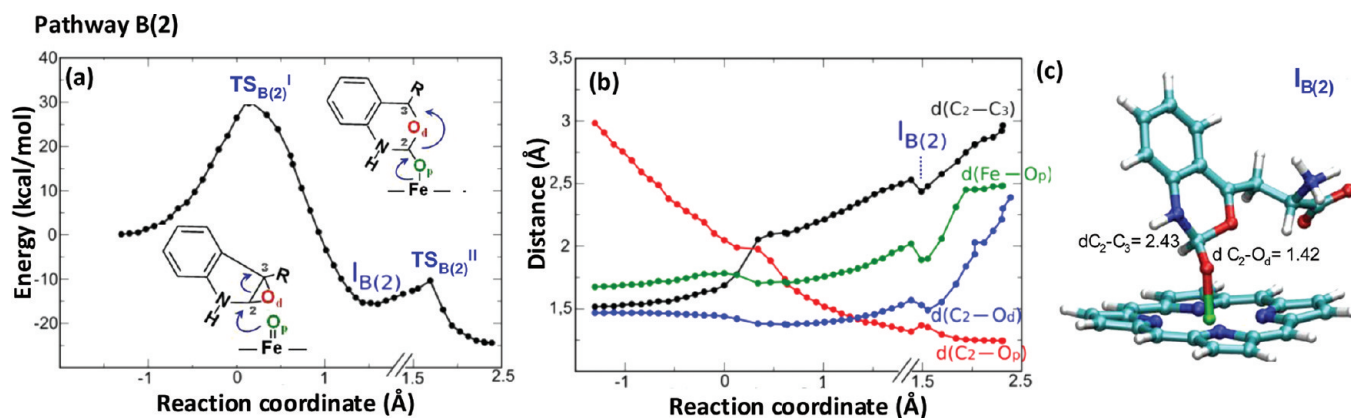


Figure 4. Energy profile (a) and distance profiles (b) as a function of the reaction coordinate along pathway B(2) in the triplet state and the structure of the associated intermediate $I_{B(2)}$ (c). The // symbol in the x -axis indicates the change in the reaction coordinate.

For pathway B(1), we evaluate the scenario that the C₂–C₃ bond cleavage precedes the ferryl oxygen attack to C₂, by using $d(C_2-C_3)$ as the starting reaction coordinate. The results (shown in Figure 3) show that the C₂–C₃ bond cleavage is homolytic. It leads to a relatively stable six-membered ring intermediate, $I_{B(1)}$, with two radicals on C₂ and C₃. In $I_{B(1)}$, the $d(C_2-C_3)$ is elongated to $\sim 2.40 \text{ \AA}$, while the $d(\text{Fe}-\text{O}_p)$, as well as all other structural parameters, remain unchanged. Furthermore, the C₂ adopts a planar sp² like structure, with the three C₂ bonds on almost the same plane. The reaction has to overcome an activation energy barrier of $\sim 31 \text{ kcal/mol}$ (to cleave the C₂–C₃ bond). The intermediate is $\sim 24 \text{ kcal/mol}$ higher in energy with respect to the ferryl and Trp–epoxide complex. To achieve the NFK product from the $I_{B(1)}$, the difference between the C₂–O_d and C₂–O_d distances [$d(C_2-\text{O}_d) - d(C_2-\text{O}_p)$] was selected as the reaction coordinate for the subsequent reaction. The data show that the ferryl oxygen attack to C₂ yields the product NFK, with a very low activation energy barrier ($\sim 2 \text{ kcal/mol}$). The low energy barrier is possibly a result of the sp² configuration of the C₂, which facilitates its nucleophilic attack by the ferryl oxygen. Like pathway A, energetic and structural parameters associated with the reaction in S and T spin states are very similar (Tables 2 and 3).

Pathway B(2): Ring Expansion Concerted with the Nucleophilic Ferryl Oxygen Addition Reaction. The activation

energy barrier of pathway B(1), like that of pathway A, is too high ($\sim 31 \text{ kcal/mol}$) to be biologically relevant. In an effort to find a lower energy trajectory of the reaction, we explored a new pathway, by using $[d(C_2-C_3) + d(\text{Fe}-\text{O}_p)] - [d(C_2-\text{O}_p) + d(C_3-\text{O}_d)]$ as the reaction coordinate, which allows the C₂–C₃ bond cleavage and ferryl oxygen attack (to C₂) to occur simultaneously (Figure 4).

The data show that the reaction leads to an intermediate, $I_{B(2)}$, via the transition state, $TS_{B(2)}^I$. In $TS_{B(2)}^I$, the C₂ adopts a trigonal bipyramidal configuration (with C₂–O_d, C₂–H, and C₂–N bonds on the same plane and the C₃ and the incoming O_p at the axial positions). On the other hand, $I_{B(2)}$ has a six-membered ring structure (Figure 4c), with a broken C₂–C₃ bond and a newly established C₂–O_p bond (black and red traces, respectively, in Figure 4b). The relative energy of the intermediate is much lower than that of pathway B(1); however, the energy barrier leading to it is as high as that of pathway B(1) ($\sim 30 \text{ kcal/mol}$). To complete the reaction, a second reaction coordinate, $d(C_2-\text{O}_d)$, was used. The data show that the reaction leads to the NFK product after crossing a small energy barrier ($\sim 10 \text{ kcal/mol}$, see Figure 4a) with the associated $TS_{B(2)}^{II}$. The reaction is associated with the breakage of the Fe–O_p and C₂–O_d bonds, as well as the change of C₂ from a sp³ to a sp² configuration. In this context, the $TS_{B(2)}^{II}$ corresponds to the last structure with

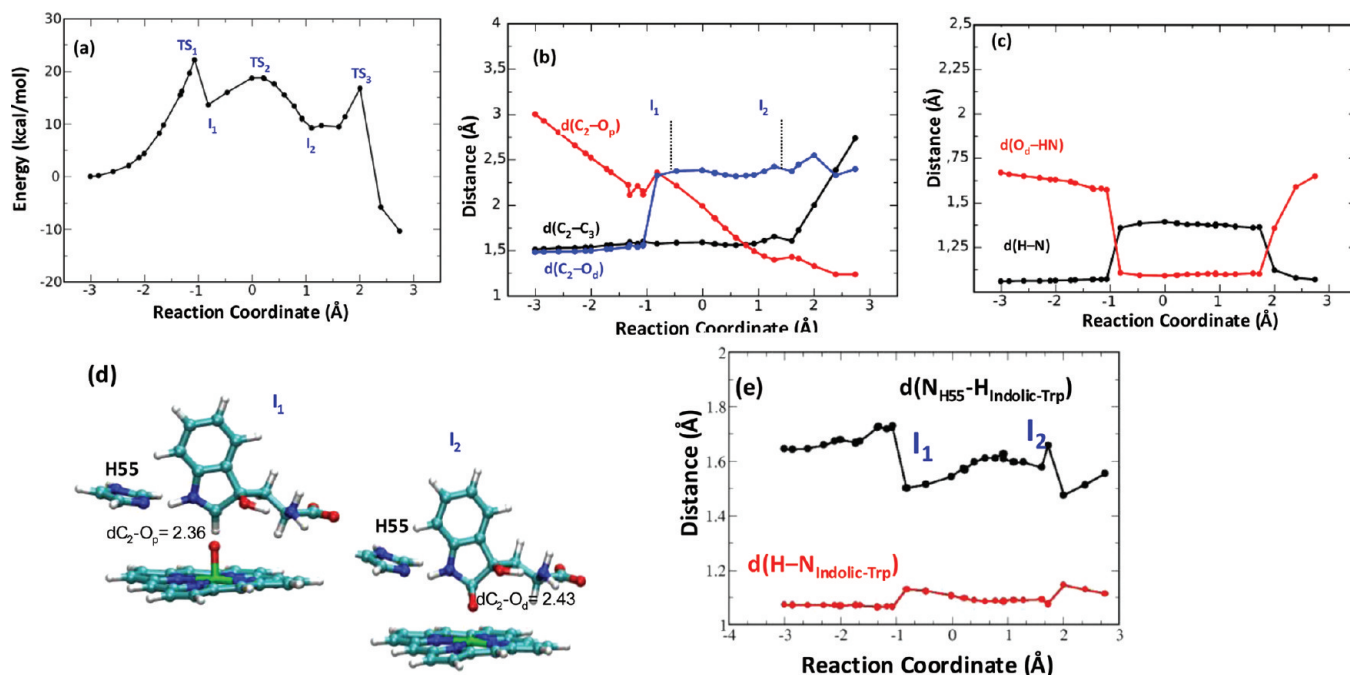


Figure 5. Energy profile (a) and distance profiles (b and c) of xcTDO as a function of the reaction coordinate along pathway C, as well as the structures of the I₁ and I₂ intermediates (d). Evolution of the distance between His5SNE and Trp indolic HN ($d(N_{H5S}-H_{\text{Indolic-Trp}})$, black line) and between the N and H atoms of the Trp indolic NH group ($d(H-N_{\text{Indolic-Trp}})$, red line) along the reaction coordinate (e).

Fe—O_p and C₂—O_d bonds character. Similar results were obtained with the S state reaction (Tables 2 and 3), although in that case the reaction goes directly to NFK without forming I_{B(2)} or any other metastable intermediate. Nonetheless, the transition state structure and the associated energy of the S state reaction are similar to those of the T state reaction. In addition, like the T state reaction, the rate-limiting step of the S state reaction involves the cleavage of the C₂—C₃ bond and the establishment of the C₂—O_p bond.

In summary, pathways A, B(1), and B(2) exhibit very similar energy barriers (~ 30 kcal/mol) in both the S and T states. They follow analogous mechanisms, where the most energy-costing event is the C₂—C₃ bond breakage, occurring either after, before, or simultaneously with the ferryl oxygen (O_p) attack to C₂. Although these pathways offer logical mechanisms accounting for the conversion of the ferryl and Trp—epoxide intermediate to NFK, the high activation energy barrier renders them less likely than previously described in pathway C.

Pathway D: Dioxetane Mechanism. To complete the analysis, we studied the possibility of ferryl oxygen attack to the epoxide to form the dioxetane intermediate (Scheme 2). Intriguingly, the results show that, after crossing a high activation energy barrier (>31 kcal/mol), the reaction proceeds directly to NFK, without populating the dioxetane intermediate. To examine the stability of the potential dioxetane intermediate, we sought to generate it from the ternary complex, by simultaneous attack of both atoms of dioxygen to the C₂=C₃ bond. We also evaluated this pathway in the Q state, as a ferrous five-coordinate high-spin heme species would be formed if a dioxetane intermediate was generated. The data show that the reaction does lead to a metastable dioxetane intermediate, but the activation energy barrier is extremely high (>50 kcal/mol) in the S, T, and Q spin states (see Table S1 in Supporting Information for details).

The high energy barrier arises from the endergonic nature of the dioxygen dissociation from the heme iron.

Due to the observation that the dioxetane intermediate is 20.1 kcal/mol higher in energy with respect to the ternary complex and that the ferryl and Trp—epoxide complex is 16.2 kcal/mol more stable than the ternary complex (Table 2), a high activation energy barrier, >36 kcal/mol, is anticipated for converting the ferryl and Trp—epoxide intermediate to the dioxetane intermediate. The high activation barrier accounts for the observation that the dioxetane intermediate could not be produced via pathway D, as the barriers for reaching the NFK product via other pathways (for example pathway A) are significantly lower. In any case, once the dioxetane is obtained it can be converted to NFK using [$d(C_2-C_3) + d(O_p-O_d)$] as the reaction coordinate, which has a small energy barrier of 5 kcal/mol (see Figure S2, Supporting Information). The TS for the reaction has an intact C₂—C₃ bond and an elongated O_p—O_d bond, to 1.83 Å (it is noted that the C₂—C₃ bond is not cleaved until the O_p—O_d bond is ruptured). In summary, the data clearly demonstrate that NFK could be produced via the dioxetane mechanism, but the activation energy for producing the dioxetane intermediate is too high to be relevant for the hIDO chemistry.

NFK Product. As expected, the NFK molecule shows a well-established C₂—O_p bond, while the C₂ and C₃ remain at a van der Waals contact distance (~ 3 Å). The S state has the lowest energy since a strong interaction is present between the iron and the C₂—O_p moiety. This interaction is diminished in the T state (which is 4.6 kcal/mol higher in energy with respect to the S state), as indicated by the longer Fe—O_p distance. The interaction is completely lost in the Q state, which is 11.5 kcal/mol higher in energy with respect to the S state (similar results were obtained for the energetic parameters of NFK in the various spin states with B3LYP; see Supporting Information for details).

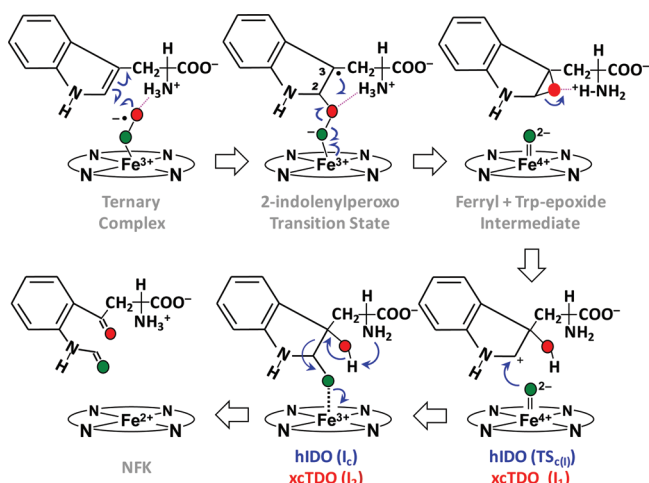
In summary, the results show that, regardless of whether the second oxygen insertion step proceeds through the T or S state, a final spin transition to the Q state must take place to completely release the product NFK, leaving the heme in a high-spin configuration ready for oxygen uptake and starting of a new enzymatic cycle.

Second Oxygen Insertion Step in xcTDO. During the preparation of the present manuscript, two theoretical studies of the xcTDO reaction mechanism were reported by Guallar et al.³² and Chung et al.,³³ using slightly different QM/MM methodologies as implemented in *Jaguar* and Gaussian-ONIOM codes, respectively. Consistently with our previous results,^{16,20} both groups showed that the first reaction step involves a direct radical addition of the ferric iron-bound superoxide to the C₂ of Trp, followed by homolytic O–O bond cleavage that leads to a ferryl and Trp–epoxide intermediate. However, different mechanisms were reported for the second reaction step from the ferryl and Trp–epoxide intermediate to the NFK product. Guallar et al.³² suggest that the product is formed by direct nucleophilic attack of the ferryl oxygen to C₂ of Trp (similar to pathway A in Scheme 2). On the other hand, in agreement with the results presented here for hIDO, Chung et al. found that the second reaction step in xcTDO is catalyzed by proton-transfer-assisted epoxide ring opening, followed by C₂–C₃ bond cleavage and back proton transfer.³³ However, instead of a two-step mechanism as we reported here for the hIDO reaction (Figure 1), a three-step mechanism, with the presence of two intermediates, was found for the xcTDO reaction.

For comparison purposes, we computed the energy profile associated with the second step of the xcTDO reaction along pathway C by using $d(C_2-C_3) + d(C_2-O_d) - 2d(C_2-O_p)$ as the reaction coordinate. The structure of the starting ferryl Trp–epoxide intermediate was obtained from our previous work.²⁰ As shown in Table 1, the structural and electronic properties of the ferryl and Trp–epoxide intermediate of xcTDO in the T state (the ground state) are similar to those of hIDO. The resulting energy profile, as well as the associated distance profiles, are shown in Figure 5. The data show that the second step of the xcTDO reaction follows a three-step mechanism, similar to that reported by Chung et al.³³ The barrier for the first step of the reaction (22 kcal/mol) separates the ferryl epoxide intermediate from the I₁ intermediate, in which the proton from the L-Trp–NH₃⁺ has been transferred to the epoxide and the epoxide ring has been opened. The reaction is followed by O_p attack to the C₂ atom, which leads to the I₂ intermediate by overcoming a 5 kcal/mol barrier. In the I₂ intermediate, the C₂–O_p bond is already formed; however, the proton is still attached to O_d, and the C₂–C₃ bond remains intact. To convert the I₂ intermediate to the NFK product, we extended the calculation by using $d(C_2-C_3)$ as the reaction coordinate, which allowed the completion of the reaction by crossing a relatively small barrier (7.3 kcal/mol). Frequency calculations support the differences between xcTDO and hIDO since for TS₁ the imaginary frequency mode only shows movement of the NH₃⁺ proton toward the epoxide oxygen, while the structure corresponding to I₁ (equivalent to TS_{C(1)} in hIDO) only shows positive frequencies confirming its intermediate state nature.

In summary, the three-step xcTDO reaction mechanism we obtained and the two intermediates thereby identified are similar to those reported by Chung et al.³³ (see Table S2, Supporting Information, for a detailed structural comparison between the intermediates obtained by us and Chung et al.³³). The fact that

Scheme 3. Ferryl-Based Mechanism of hIDO Derived from QM/MM Calculations^a



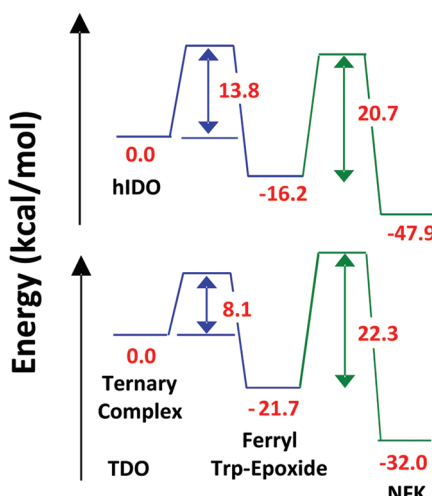
^a The second oxygen insertion (from the ferryl + Trp–epoxide intermediate to the NFK product) is derived from the data shown in Figures 1 and 5.

the same reaction mechanism is observed with different exchange correlation functionals (PBE⁴⁰ vs B3LYP⁵⁵), different QM/MM implementations (Hybrid³⁹ vs ONION^{56,57}), and different strategies for locating and computing the TS state energies (restrained energy profiles⁵⁸ vs TS searching⁵⁹) confirms the reliability of our work. It also strongly supports the validity of the sequential oxygen insertion mechanism in both IDO and TDO families of enzymes (with subtle differences as discussed above). It is noteworthy that the sequential oxygen insertion mechanism is also supported by the recent observation that both IDO and TDO are able to produce a cyclic amino acetal species as a side product derived from the ring opening of the epoxide intermediate, followed by a subsequent attack of the amino group to C₂.²¹

■ DISCUSSION

The overall ferryl-based mechanism for the hIDO and xcTDO enzymatic reaction, as derived from our previous^{16,20} and current work, is summarized in Scheme 3. Two movie clips resulting from the QM/MM studies are provided in the Supporting Information. In the proposed mechanism, the reaction is initiated by radical addition of the ferric iron-bound superoxide to the C₂=C₃ bond of Trp to form a ferryl and Trp–epoxide intermediate, via a 2-indolenylperoxo radical transition state. For hIDO, the ensuing reaction is then initiated by proton transfer from Trp–NH₃⁺ to the epoxide oxygen, which allows opening of the epoxide ring and the attack of the ferryl oxygen to the C₂ of Trp. This gives origin to a heme-iron bound intermediate, I_C, which subsequently converts to the NFK product, following C₂–C₃ bond cleavage and the associated back proton transfer from oxygen to Trp–NH₂. A similar mechanism was observed for the xcTDO reaction, except that: for the first oxygen attack, the radical nature of the iron-bound superoxide is not undoubtedly established (since the superoxide bears zero spin density in the singlet state), and the second transition state, TS_{C(1)}, observed in hIDO is significantly stabilized in xcTDO and hence appears as an intermediate (I₁ in Scheme 3) instead of a transition state.

Scheme 4. Energetic Parameters Associated with the Consecutive Two-Step Oxygen Insertion Reactions of hIDO and xcTDO along the Triplet Reaction Trajectory^a



^a The energy barriers indicated correspond to the overall values for the first and second oxygen additions to the substrate, L-Trp.

The presence of the I₁ intermediate in the xcTDO reaction, but not the hIDO reaction, highlights the subtle differences between the xcTDO and hIDO. For the xcTDO reaction, proton transfer from Trp-NH₃⁺ to the epoxide results in the opening of the epoxide ring, leading to the intermediate I₁. In hIDO, the partial carbocation character of C₂ ($qC_2 = 0.229\text{ e}$) in TS_{C(1)} resulting from the epoxide ring-opening reaction cannot be stabilized by the protein environment, hence it appears as a transition state. This observation is consistent with the data shown in Figure S1 in the Supporting Information, demonstrating that proton transfer from Trp-NH₃⁺ to the epoxide does not yield a stable intermediate state, unless O_p attack to C₂ occurs concertedly. In xcTDO, the developed positive charge on the C₂ atom in the I₁ intermediate is delocalized in the indolic ring, as indicated by the almost neutral charge on C₂ and the positive charge of the indolic N of 0.435 e (Table 4). This effect can be interpreted in terms of the formation of a partial double bond between the C₂ and N atoms, giving the C₂ atom an sp²-like character. This charge rearrangement can be achieved in xcTDO, but not hIDO, as in the former the indoleamine N-H bond is strongly polarized by H55. It is important to note that H55 is replaced by S167 in hIDO, but S167 is too far to interact with the indoleamine group and hydrogen bonded to the heme carboxylate. The polarization effect induced by H55 in xcTDO is evident from an analysis of the corresponding hydrogen bond interaction along the reaction. Analysis of the corresponding structural parameters (Figure 5e) shows that after crossing TS₁ to reach I₁ the N-H bond is enlarged to 1.131 Å (while it is 1.031 Å in the TS_{C(1)} of hIDO), and the H55Nε-TrpH_{NH} hydrogen bond distance is decreased by 0.2 Å. This effect lasts until TS₂, after which the distances return to their starting values. Therefore, between I₁ and TS₂ the Trp epoxide shows a partial proton transfer to H55. As an alternative possible explanation for the observed difference, we performed energy decomposition analysis along the reaction. The results show that the QM/MM interaction energy which captures most of the electrostatic stabilization provided by the enzyme is similar in both proteins cases and

does not change significantly during the reaction, ruling out preferential electrostatic stabilization of I₁ in xcTDO (except for the discussed role of H55 which is included in the QM system) against TS_{C(1)} in hIDO. The important role of H55 in the xcTDO reaction is consistent with mutagenesis studies which showed that its replacement diminishes, but not completely abolishes, its catalytic activity.^{4,7,27} Furthermore, the hydrogen bond between the NH₃⁺ and the epoxide O_d is shorter in the ferryl-Trp-epoxide complex of xcTDO, as compared to that of hIDO (2.537 vs 2.695 Å between the two heavy atoms), indicating that the protein matrix in xcTDO accommodates better the ammonium group, which may offer additional stabilization of the I₁ intermediate of xcTDO.

In Scheme 4, we summarize the energetic parameters associated with the consecutive two-step oxygen insertion reactions of hIDO and xcTDO along the T state trajectory. The data indicate that the potential energy barriers are very similar for the two enzymes, with the first energy barrier lower than the second energy barrier. The hIDO results nicely account for the fact that the ferryl intermediate can be accumulated for experimental observations.¹⁶ Intriguingly, our earlier data showed that the ferryl intermediate of hTDO, in contrast to hIDO, cannot be accumulated for detection,^{16,20} suggesting that the reaction energy profile of the human enzyme hTDO is distinct from that computed in xcTDO shown below. Consistent with this scenario, previous data show that the k_{cat} for L-Trp is 10-fold higher in xcTDO as compared to hTDO, and in contrast, while xcTDO presents no activity toward D-Trp, hTDO exhibits significant activity toward the D-isomer.³ A definite explanation for the observed differences in human and bacterial TDO is still missing and will require further study.

In summary, the present data not only reveal the lowest energy pathway of the hIDO and xcTDO reaction but also provide mechanistic insights ruling out the widely accepted base-catalyzed mechanism for Trp enzymatic dioxygenation.^{2,29} Our data show that the initial step of the reaction is made possible by three key factors: (1) charge transfer from the heme to the heme-bound O₂, which activates the dioxygen for the radical addition reaction of O₂ to Trp; (2) the regio-orientation of the heme-bound O₂ with respect to the C₂=C₃ of Trp, which allows the addition of the dioxygen to C₂, instead of C₃; (3) the hydrogen bond interaction between the heme-bound O₂ and Trp-NH₃⁺, which stabilizes the partial negative charge on the alkylperoxo transition state. As such, deprotonation of the indoleamine group of Trp is not required for the reaction. The second step of the reaction, on the other hand, is promoted by the proper positioning of Trp-NH₃⁺ with respect to O_d of the epoxide, as well as the temporary proton transfer from the former to the latter.

CONCLUSIONS

Using state-of-the-art QM/MM calculations, we have revealed a new two-step ferryl-based mechanism of hIDO and xcTDO as illustrated in Scheme 4. Our data demonstrated that the NH₃⁺ group of Trp plays a critical role by acting as an acid catalyst in facilitating the subsequent ring-opening reaction of the Trp-epoxide and the ferryl oxygen addition to the indole ring of Trp.

ASSOCIATED CONTENT

S Supporting Information. Details on the computational methods, results for the Proton transfer-assisted epoxide ring-opening

reaction and dioxetane formation in hIDO, analysis of TrpNH His55 hydrogen bond along the reaction and effect of the chosen reaction coordinate in xcTDO, energy profiles calculated with B3LYP functional for pathway C in hIDO and xcTDO, movie clips describing the two steps of the oxygen insertion reaction carried out by hIDO, and .zip file containing all coordinates of QM atoms for all stable, transition states and intermediates for both enzymes (hIDO and xcTDO). This material is available free of charge via the Internet at <http://pubs.acs.org>.

AUTHOR INFORMATION

Corresponding Author

*E-mail: dario@qi.fcen.uba.ar; marcelo@qi.fcen.uba.ar.

Present Addresses

[†]German Research School for Simulation Sciences, FZ-Juelich and RWTH Aachen, Juelich, Germany.

ACKNOWLEDGMENT

This work was partially supported by grants from Universidad de Buenos Aires 08-X625 to M.A.M. and 08-X074 to D.A.E., ANPCYT 07-1650 to M.A.M., and 06-25667 to D.A.E., Conicet PIP 01207 to D.A.E. It was also supported by National Institutes of Health grant GM086482 and National Science Foundation Grant No. 1026788 to S.-R.Y. and National Institute of Health Molecular Biophysics Training Grant GM008572 to A.L.-B. D.A.E. and M.A.M. are members of CONICET. Computer power was gently provided by Cecar at FCEN, UBA, and Cluster MCG at UNC. LC thanks CONICET for the postdoctoral fellowship.

REFERENCES

- (1) Hayaishi, O. *J. Biochem.* **1976**, *79*, 13.
- (2) Sono, M.; Roach, M. P.; Coulter, E. D.; Dawson, J. H. *Chem. Rev.* **1996**, *96*, 2841.
- (3) Batabyal, D.; Yeh, S. R. *J. Am. Chem. Soc.* **2007**, *129*, 15690.
- (4) Batabyal, D.; Yeh, S.-R. *J. Am. Chem. Soc.* **2009**, *131*, 3260.
- (5) Zhang, Y.; Kang, S. A.; Mukherjee, T.; Bale, S.; Crane, B. R.; Begley, T. P.; Ealick, S. E. *Biochemistry* **2007**, *46*, 145.
- (6) Forouhar, F.; Anderson, J. L. R.; Mowat, C. G.; Vorobiev, S. M.; Hussain, A.; Abashidze, M.; Bruckmann, C.; Thackray, S. J.; Seetharaman, J.; Tucker, T.; Xiao, R.; Ma, L.-C.; Zhao, L.; Acton, T. B.; Montelione, G. T.; Chapman, S. K.; Tong, L. *Proc. Natl. Acad. Sci. U.S.A.* **2007**, *104*, 473.
- (7) Chauhan, N.; Basran, J.; Efimov, I.; Svistunenko, D. A.; Seward, H. E.; Moody, P. C. E.; Raven, E. L. *Biochemistry* **2008**, *47*, 4761.
- (8) Leeds, J. M.; Brown, P. J.; McGeehan, G. M.; Brown, F. K.; Wiseman, J. S. *J. Biol. Chem.* **1993**, *268*, 17781.
- (9) Takikawa, O. *Biochem. Biophys. Res. Commun.* **2005**, *338*, 12.
- (10) Greengard, O.; Feigelson, P. J. *Biol. Chem.* **1962**, *237*, 1903.
- (11) Friberg, M.; Jennings, R.; Alsarraj, M.; Dessureault, S.; Cantor, A.; Extermann, M.; Mellor, A. L.; Munn, D. H.; Antonia, S. J. *Int. J. Cancer* **2002**, *101*, 151.
- (12) Muller, A. J.; DuHadaway, J. B.; Donover, P. S.; Sutanto-Ward, E.; Prendergast, G. C. *Nat. Med.* **2005**, *11*, 312.
- (13) Lob, S.; Konigsrainer, A.; Rammensee, H.-G.; Opelz, G.; Terness, P. *Nat. Rev. Cancer* **2009**, *9*, 445.
- (14) Liu, X.; Newton, R. C.; Friedman, S. M.; Scherle, P. A. *Curr. Cancer Drug Targets* **2009**, *9*, 938.
- (15) Katz, J. B.; Muller, A. J.; Prendergast, G. C. *Immunol. Rev.* **2008**, *222*, 206.
- (16) Lewis-Ballester, A.; Batabyal, D.; Egawa, T.; Lu, C.; Lin, Y.; Marti, M. A.; Capece, L.; Estrin, D. A.; Yeh, S. R. *Proc. Natl. Acad. Sci. U.S.A.* **2009**, *106*, 17371.
- (17) Capece, L.; Arrar, M.; Roitberg, A. E.; Yeh, S.-R.; Marti, M. A.; Estrin, D. A. *Proteins: Struct., Funct., Bioinf.* **2010**, *78*, 2961.
- (18) Chauhan, N.; Thackray, S. J.; Rafice, S. A.; Eaton, G.; Lee, M.; Efimov, I.; Basran, J.; Jenkins, P. R.; Mowat, C. G.; Chapman, S. K.; Raven, E. L. *J. Am. Chem. Soc.* **2009**, *131*, 4186.
- (19) Davydov, R. M.; Chauhan, N.; Thackray, S. J.; Anderson, J. L. R.; Papadopoulou, N. D.; Mowat, C. G.; Chapman, S. K.; Raven, E. L.; Hoffman, B. M. *J. Am. Chem. Soc.* **2010**, *132*, 5494.
- (20) Capece, L.; Lewis-Ballester, A.; Batabyal, D.; Di Russo, N.; Yeh, S.-R.; Estrin, D.; Marti, M. *J. Biol. Inorg. Chem.* **2010**, *15*, 811.
- (21) Basran, J.; Efimov, I.; Chauhan, N.; Thackray, S. J.; Krupa, J. L.; Eaton, G.; Griffith, G. A.; Mowat, C. G.; Handa, S.; Raven, E. L. *J. Am. Chem. Soc.* **2011**, *133*, 16251.
- (22) Lu, C.; Lin, Y.; Yeh, S.-R. *J. Am. Chem. Soc.* **2009**, *131*, 12866.
- (23) Samelson-Jones, B. J.; Yeh, S. R. *Biochemistry* **2006**, *45*, 8527.
- (24) Terentis, A. C.; Thomas, S. R.; Takikawa, O.; Littlejohn, T. K.; Truscott, R. J. W.; Armstrong, R. S.; Yeh, S.-R.; Stocker, R. *J. Biol. Chem.* **2002**, *277*, 15788.
- (25) Yanagisawa, S.; Yotsuya, K.; Hashiwaki, Y.; Horitani, M.; Sugimoto, H.; Shiro, Y.; Appelman, E. H.; Ogura, T. *Chem. Lett.* **2010**, *39*, 37.
- (26) Sugimoto, H.; Oda, S.-i.; Otsuki, T.; Hino, T.; Yoshida, T.; Shiro, Y. *Proc. Natl. Acad. Sci. U.S.A.* **2006**, *103*, 2611.
- (27) Thackray, S. J.; Bruckmann, C.; Anderson, J. L. R.; Campbell, L. P.; Xiao, R.; Zhao, L.; Mowat, C. G.; Forouhar, F.; Tong, L.; Chapman, S. K. *Biochemistry* **2008**, *47*, 10677.
- (28) Efimov, I.; Basran, J.; Thackray, S. J.; Handa, S.; Mowat, C. G.; Raven, E. L. *Biochemistry* **2011**, *50*, 2717.
- (29) Hamilton, G. A. *Adv. Enzymol. Relat. Areas Mol. Biol.* **1969**, *32*, 55.
- (30) Ronsein, G. E.; Oliveira, M. C. B.; Miyamoto, S.; Medeiros, M. H. G.; Di Mascio, P. *Chem. Res. Toxicol.* **2008**, *21*, 1271.
- (31) Chung, L. W.; Li, X.; Sugimoto, H.; Shiro, Y.; Morokuma, K. *J. Am. Chem. Soc.* **2008**, *130*, 12299.
- (32) Guallar, V.; Wallrapp, F. H. *Biophys. Chem.* **2010**, *149*, 1.
- (33) Chung, L. W.; Li, X.; Sugimoto, H.; Shiro, Y.; Morokuma, K. *J. Am. Chem. Soc.* **2010**, *132*, 11993.
- (34) Brady, F. O.; Feigelson, P. J. *Biol. Chem.* **1975**, *250*, 5041.
- (35) Fu, R.; Gupta, R.; Geng, J.; Dornevil, K.; Wang, S.; Zhang, Y.; Hendrich, M. P.; Liu, A. *J. Biol. Chem.* **2011**, *286*, 26541.
- (36) Morris, G. M.; Goodsell, D. S.; Halliday, R. S.; Huey, R.; Hart, W. E.; Belew, R. K.; Olson, A. J. *J. Comput. Chem.* **2005**, *19*, 1639.
- (37) Pearlman, D. A.; Case, D. A.; Caldwell, J. W.; Ross, W. S.; Cheatham, T. E.; DeBolt, S.; Ferguson, D.; Seibel, G.; Kollman, P. *Comput. Phys. Commun.* **1995**, *91*, 1.
- (38) Marti, M. A.; Capece, L.; Bidon-Chanal, A.; Crespo, A.; Guallar, V.; Luque, F. J.; Estrin, D. A. *Methods Enzymol.* **2008**, *437*, 477.
- (39) Crespo, A.; Scherlis, D. A.; Marti, M. A.; Ordejon, P.; Roitberg, A. E.; Estrin, D. A. *J. Phys. Chem. B* **2003**, *107*, 13728.
- (40) Perdew, J. P.; Burke, K.; Ernzerhof, M. *Phys. Rev. Lett.* **1996**, *77*, 3865.
- (41) Shaik, S.; Kumar, D.; de Visser, S. I. P.; Altun, A.; Thiel, W. *Chem. Rev.* **2005**, *105*, 2279.
- (42) Senn, H. M.; Thiel, W. *Curr. Opin. Chem. Biol.* **2007**, *11*, 182.
- (43) Ranaghan, K. E.; Mulholland, A. *J. Int. Rev. Phys. Chem.* **2010**, *29*, 65.
- (44) Capece, L.; Marti, M. A.; Crespo, A.; Doctorovich, F.; Estrin, D. A. *J. Am. Chem. Soc.* **2006**, *128*, 12455.
- (45) Marti, M. A.; Crespo, A.; Bari, S. E.; Doctorovich, F. A.; Estrin, D. A. *J. Phys. Chem. B* **2004**, *108*, 18073.
- (46) Marti, M. A.; Capece, L.; Crespo, A.; Doctorovich, F.; Estrin, D. A. *J. Am. Chem. Soc.* **2005**, *127*, 7721.
- (47) Crespo, A.; Marti, M. A.; Kalko, S. G.; Morreale, A.; Orozco, M.; Gelpi, J. L.; Luque, F. J.; Estrin, D. A. *J. Am. Chem. Soc.* **2005**, *127*, 4433.

- (48) Bikiel, D. E.; Boechi, L.; Capece, L.; Crespo, A.; De Biase, P. M.; Di Lella, S.; González Lebrero, M. C.; Martí, M. A.; Nadra, A. D.; Perissinotti, L. L.; Scherlis, D. A.; Estrin, D. A. *Phys. Chem. Chem. Phys.* **2006**, *8*, 5611.
- (49) Perissinotti, L. L.; Martí, M. A.; Doctorovich, F.; Luque, F. J.; Estrin, D. A. *Biochemistry* **2008**, *47*, 9793.
- (50) Crespo, A.; Martí, M. A.; Roitberg, A. E.; Amzel, L. M.; Estrin, D. A. *J. Am. Chem. Soc.* **2006**, *128*, 12817.
- (51) Pople, J. A. et al. *Gaussian 03*; Gaussian, Inc.: Wallingford, CT, 2004.
- (52) Guallar, V.; Harris, D. L.; Batista, V. S.; Miller, W. H. *J. Am. Chem. Soc.* **2002**, *124*, 1430.
- (53) Rovira, C.; Fita, I. *J. Phys. Chem. B* **2003**, *107*, 5300.
- (54) Chen, H.; Hirao, H.; Derat, E.; Schlichting, I.; Shaik, S. *J. Phys. Chem. B* **2008**, *112*, 9490.
- (55) Becke, A. D. *J. Chem. Phys.* **1993**, *98*, 1372.
- (56) Maseras, F.; Morokuma, K. *J. Comput. Chem.* **1995**, *16*, 1170.
- (57) Humbel, S.; Sieber, S.; Morokuma, K. *J. Chem. Phys.* **1996**, *105*, 1959.
- (58) Martí, M. A.; Capece, L.; BidonChanal, A.; Crespo, A.; Guallar, V.; Luque, F. J.; Estrin, D. A.; Robert, K. P. Nitric Oxide Reactivity with Globins as Investigated Through Computer Simulation. In *Methods Enzymology*; Academic Press: New York, 2008; Vol. 437, p 477.
- (59) Vreven, T.; Frisch, M. J.; Kudin, K. N.; Schlegel, H. B.; Morokuma, K. *Mol. Phys.* **2006**, *104*, 701.